SLAC-PUB-3597
March 1985
(A)

MEASUREMENTS OF ULTIMATE ACCELERATING GRADIENTS IN THE SLAC DISK-LOADED STRUCTURE*

J. W. WANG AND G. A. LOEW
Stanford Linear Accelerator Center
Stanford University, Stanford, California 94305

Introduction

This paper is a status report on an on-going program at SLAC to study accelerator structures under high-gradient electric field conditions. The study is a part of a much broader program dealing with future linear colliders. The accelerating gradient that might be achievable in such machines is a crucial parameter because once the beam energy is selected, the gradient determines the length of the linac and directly or indirectly affects the choice of many other parameters[1] such as frequency, energy consumption, size and number of RF sources, alignment, wakefield control, etc.

The experiments done so far at SLAC deal with a conventional disk-loaded accelerator section of the constant-gradient type running at 2856 MHz. The original objective was to reach an accelerating gradient of at least 100 MV/m. The accelerating gradient at which the SLAC disk-loaded waveguide operates routinely is ~ 9 MV/m (with 36 MW klystrons feeding four 3 m sections without SLED) and ~ 12 MV/m with SLED I (2.5 μsec pulse). With 50 MW tubes and SLED II (5 μsec pulse) the gradient is presently being increased to over 20 MV/m. To reach 100 MV/m in a conventional 3 m constant-gradient section without SLED, one would need a klystron with a peak power output of 900 MW. Since such a tube is not available, we decided to use a short standing-wave section in which the resonant fields can build up. The design criteria for this section, the fabrication, matching and tuning, the experimental set-up and the results are described below.

Design Criteria

Standing-wave accelerators are generally built in the π-mode or some variation thereof so that both forward and reflected waves contribute to the acceleration of a synchronous particle. In the case of this experiment, however, our primary goal was not to accelerate electrons but rather, to test a $2\pi/3$-mode SLAC-type of section to its maximum attainable field. We took advantage of the availability of short six-cavity stacks, already brazed onto a coupler, to speed up the experiment (see Fig. 1). These stacks were actually the input and output segments of the SLAC 3 m sections. The complete sections consist of a total of 84 regular cavities and two coupler cavities. In the original manufacturing process, the short stacks were brazed separately and then joined onto the center portion of the section (74 cavities). We chose the output stack because it has a lower group velocity and a higher field intensity for a given power input, and we capped it off with a disk at the end opposite to the coupler to make it resonant. Thus our standing-wave section consists of seven cavities.

The conceptual passage from standing waves to traveling waves and vice versa has been studied in detail elsewhere.[2] One of the main differences is that in the traveling wave the E and H fields are in time phase whereas in the standing wave they are in time quadrature. To calculate the field parameters in our standing-wave section conservatively, we used the SUPERFISH program on the lowest field cavity (No. 79) of the constant-gradient stack. The calculation[2] is performed for Neuman-Neuman boundaries across one and one-half cavity ($L = 5.25$ cm) and the normalizing condition given by

$$(\int_0^L | E_z(z) | dz)/L = 1 \text{ MV/m}.$$

The cavity dimensions and calculated field parameters are summarized in Table I below.

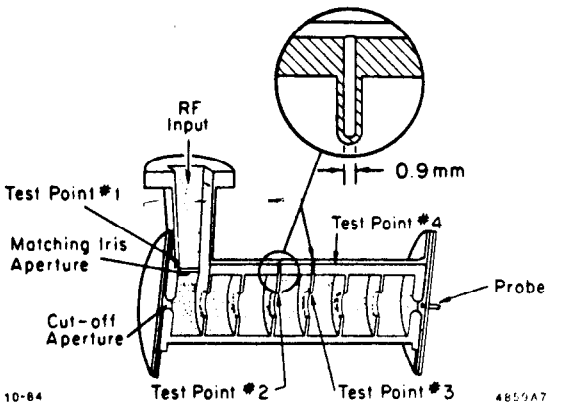

Fig. 1. Resonant structure used for these experiments. Test points indicate locations of thermocouples used to monitor temperatures during operation.

Table I

Iris diameter $2a$	1.99 cm
Cavity diameter $2b$	8.192 cm
Traveling-wave r/Q per unit length	47.4 Ω/cm
Q	13,712
Resonant frequency f	2855.76 MHz
Standing-wave R/Q for length $L = 5.25$ cm	124.4 Ω
$\mid \int_0^L E_z(z) e^{j(\omega z/c)} dz \mid$	0.038 MV
Energy stored W	6.453×10^{-4} J
Power dissipated $P_D = \omega W/Q$	844 W
Max. axial field at $z = 0$, $\mid E_{z,SW} \mid_{max}$	1.916 MV/m
Max. surface field at disk edge, $\mid E_{s,SW} \mid_{max}$	2.81 MV/m
Average accelerating field $\bar{E}_{acc}$	0.723 MV/m
$\mid E_{z,SW} \mid_{max} / \bar{E}_{acc}$	2.65
$\mid E_{s,SW} \mid_{max} / \bar{E}_{acc}$	3.89

Note that the standing-wave R/Q is half of that for the traveling wave because twice the energy is stored for the same accelerating field. Note also that the above $\mid E \mid_{max}$ are maxima reached by the standing wave which can be viewed as the sum of two traveling waves, one traveling to the right, the other to the left. For a particle traveling to the right on crest at the velocity of light, the first wave alone produces acceleration. Given these conditions, we see that to create fields in our standing-wave structure that simulate accelerating fields of 100 MV/m in a traveling-wave structure, it is enough to supply the 1-1/2 cavity cell with that power which yields $\bar{E}_{acc} = 50$ MV/m. For our stack of seven cavities, that power was calculated to be 17.06 MW. Note that the 100 MV/m condition is only fulfilled in every third cell, as we will see illustrated below. The equivalent traveling-wave fields for a power input P_{in} in MW are:

*Work supported by the Department of Energy, contract DE-AC03-76SF00515.

Poster Paper Presented at the 1985 Particle Accelerator Conference
Vancouver, B.C., Canada, May 13-16, 1985

$$\text{Accelerating axial fields} \quad E_{z,TW} = \sqrt{\frac{P_{in}}{17.06}} \times 100 \text{ MV/m} \qquad (1a)$$

$$\text{Surface fields} \quad E_{s,TW} = \sqrt{\frac{P_{in}}{17.06}} \times 194.5 \text{ MV/m} \quad . \qquad (1b)$$

Fabrication, Matching and Tuning

Four mechanical modifications were made to complete the fabrication of the standing-wave section. The first was to braze sixteen (instead of the usual eight) cooling tubes around the section to improve the cooling. The second was to drill small holes (by EDM) into the wall and disks of the section (see Fig. 1) to insert thermocouples for temperature monitoring. The third was to terminate the last cylinder (cavity 79) with a disk of diameter $2a = 0.7617$ in., and to cap off both ends with 1.2 mm stainless steel plates to provide vacuum seals. The fourth was to braze an extra matching iris into the input coupler to critically couple the section for maximum power delivery. A coupling coefficient of $\beta = 1.08$ was obtained for an iris opening of 0.78 in. Tuning of the section was done by the usual nodal shift technique.[3] A dielectric bead was then pulled along the axis of the section and the power reflected by the bead was plotted, as shown in Fig. 2. Note that cavities 83 and 80 are the ones that reach maximum field; the coupler and the other cavities do not.

Experimental Set-Up and Results

The RF system used to perform the measurements consists of a low-level variable frequency oscillator, a pin-diode modulator, a pulsed driver amplifier and a SLAC XK-5 klystron which supplies up to about 30 MW of peak power to the accelerator section. The variable frequency oscillator is needed because the temperature of the section changes as the input power is increased, and the oscillator has to be retuned to keep the section resonant. A 60 ℓ/sec vacion pump is used directly on the section, a residual gas analyser monitors the gasses emitted during RF processing and operation, and a multipoint thermocouple reader gives the temperature of the section at the points shown in Fig. 1. The cooling water flow is set at 15 gpm with an input temperature of 83° F which corresponds to a resonant frequency of ~ 2856.8 MHz at low power level.

Two series of RF tests have been conducted so far, the first in Spring 1984, the second in Spring 1985. Before the first series, the section was baked at roughly 250° C for 36 hours. The pressure after bake was 10^{-8} Torr. The RF was then turned on gradually to let the section outgas. Only minor RF processing was required up to 28 MW (see the pulses shown in Fig. 3a). The pressure was then roughly 2×10^{-7} Torr. When the input power was somewhat abruptly increased to its maximum attainable, namely 30.2 MW, the pressure rose to about 8×10^{-7} Torr and the section exhibited the breakdown shown in Fig. 3b. After some further processing and pumpdown back to 2×10^{-7} Torr, the breakdown disappeared and the stable condition shown in Fig. 3c was obtained without difficulty. The wiggles within the pulse were probably due to a combination of ripple from the PFN in the modulator and internal reflections within the section as it filled and emptied. The outgassing as observed by the RGA revealed only the presence of some water, nitrogen, fluorine and methane.

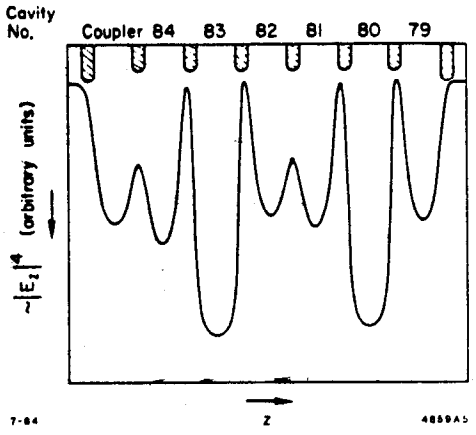

Fig. 2. Power reflected by bead as a function of axial position (in arbitrary units). This power, if it were measured with a perfect square-law crystal, would be proportional to $|E_z|^4$ because the reflection coefficient of the bead is proportional to $|E_z|^2$ and the reflected power scales as the square of the reflection coefficient.

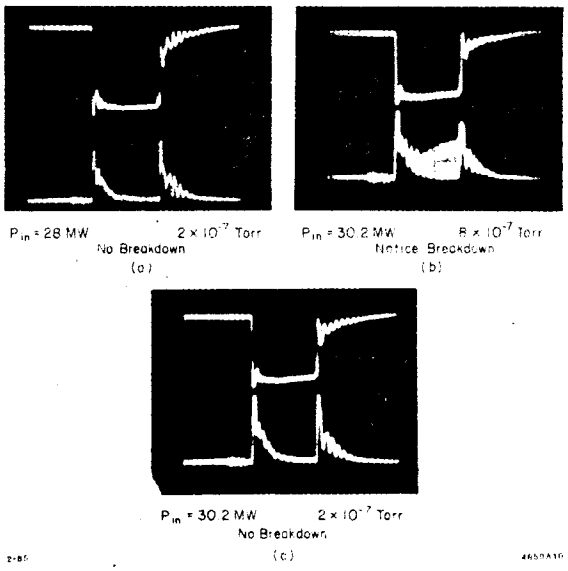

Fig 3. Forward (top) and reflected (bottom) rf wave shapes under various input conditions.

Using expressions (1), the maximum equivalent traveling-wave accelerating and surface fields for these conditions were:

$$E_{z,TW} \sim 133 \text{ MV/m} \qquad E_{s,TW} \sim 259 \text{ MV/m} \quad .$$

The klystron output power could not be increased further. Note that the above fields were reached and maintained after the standing-wave structure was fully charged, roughly 1.5 μsec into the 2.5 μsec pulse. The results reported here are similar to those given for the single cavity tests described in Ref. 4.

Figure 4 shows the temperatures monitored in the section as a function of average power dissipated.[5] All variations appear to be linear. Test points 2 and 3 are in successive disks, and test point 4 is in the outer wall. As we see, test point 2 rose twice as fast as test point 3 because the fields in cavity 83 were higher than those in cavity 82. This, of course, would not happen in a traveling-wave structure because all cavities would undergo the same excitation and power dissipation. Figure 4 also shows the resonant frequency of the section as a function of average power dissipated. Note that the variation is not quite linear.

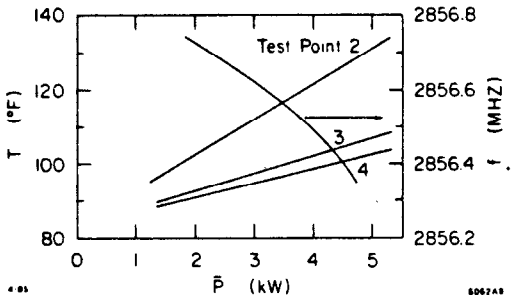

Fig. 4. Temperatures for the test points shown in Fig. 1 and resonant frequency, both as a function of average power dissipated in accelerator section.

During the above tests, even though RF breakdown was easy to overcome, considerable x-ray radiation was observed in the concrete vault around the section at the high power levels. Field emission was clearly present and the resulting radiation as the electrons were accelerated in the section and hit the end-plates could be monitored as a function of time within the pulse by means of a photodetector connected to an oscilloscope. The radiation had the same general time-variation as the fields. After completion of this first series of tests, blue spots due to heating from the radiation could be seen externally on the axis of both stainless steel end-plates.

In an attempt to refine the measurements, the end-plate at the end of the section opposite to the coupler was removed and fitted with two coaxial electric probes (see Fig. 5). The purpose of these probes was to monitor both the RF and the field-emitted current at that end. During the subsequent nine months, the high-power klystron was used for RF superconducting tests and the drive system was entirely rebuilt. In March 1985, after another period of two weeks during which the section was rebaked at 250° C, the RF tests resumed. This time, another thermocouple was affixed next to one of the coaxial feedthroughs. As the power input approached 19 MW peak at 120 pps, some RF breakdown became apparent and increased x-ray radiation was observed inside and outside of the vault. Within a few minutes, the temperature of the end-plate rose to 400° C and before the RF power could be turned down, the section vacuum went up to air. Observation subsequently revealed that the 1.2 mm stainless steel end-plate exhibited a well-centered 1 mm diameter hole (see Fig. 5). The evidence is that an RF focussed beam of electrons captured and accelerated up to a maximum of 10 MeV with an average power of up to 100 W melted the stainless steel[6] which then imploded and coated several of the adjacent disks. A subsequent measurement, however, showed no degradation of the cavity Q at low power. It is not clear why the radiation was so much worse during this second series of tests. As this paper is being written, the section is being fitted with new copper end-plates (for improved thermal conductivity) comprising thinned-down axial "windows" (0.015 in. thick) to permit extraction and characterization of the "dark" beam.

Fig. 5. Stainless steel end-plate with probes, showing 1 mm hole produced by "dark" beam.

Acknowledgements

The authors are indebted to H. Deruyter who helped with the tuning and matching of the section, and to J. Zamzow who helped with the overall installation and the RF power measurements. The authors also wish to thank W. Jacopi who was responsible for many of the details of the fabrication, E. Garwin who provided useful advice on vacuum questions, and to R. Miller for useful discussions.

References

1. See for example R. B. Neal, "Accelerator Parameters for an e^+e^- Super Linear Collider," SLAC/AP-7, 1983.
2. G. A. Loew, R. H. Miller, R. A. Early and K. L. Bane, "Computer Calculations of Traveling-Wave Periodic Structure Properties," IEEE Trans. Nucl. Sci., NS-26, p. 3701, 1979; also SLAC-PUB 2295.
3. "The Stanford Two-Mile Accelerator," R. B. Neal, Editor (W. A. Benjamin, Inc., New York, 1968), pp. 95-162.
4. E. Tanabe, "Voltage Breakdown in S-Band Linear Accelerator Cavities," IEEE Trans. Nucl. Sci., NS-30, p. 3351, 1983.
5. For details of how this power is calculated, see SLAC-AP/26 with private communication by Z. D. Farkas.
6. Calculations made by R. H. Miller, D. R. Wals and R. C. McCall at SLAC.